Reinforced Ni(II)-cyclam derivatives as dual $^{1}H/^{19}F$ MRI probes[i]

Rosa Pujales-Paradela[a], Tanja Savić[b], Isabel Brandariz[a], Paulo Pérez-Lourido[c], Goran Angelovski[b], David Esteban-Gómez[a*], and Carlos Platas-Iglesias[a†]

[a] Centro de Investigacións Científicas Avanzadas (CICA) and Departamento de Química, Facultade de Ciencias, Universidade da Coruña, 15071 A Coruña, Galicia, Spain

[b] MR Neuroimaging Agents, Max Planck Institute for Biological Cybernetics, Tuebingen, Germany

[c] Departamento de Química Inorgánica, Facultad de Ciencias, Universidade de Vigo, As Lagoas, Marcosende, 36310 Pontevedra, Spain

Chemical Communications, volume 55, issue 28, pages 4115–4118, 11 April 2019
Submitted 11 February 2019, accepted 8 March 2019, first published 11 March 2019

How to cite:

R. Pujales-Paradela, T. Savić, I. Brandariz, P. Pérez-Lourido, G. Angelovski, D. Esteban-Gómez and C. Platas-Iglesias, Reinforced Ni(II)-cyclam derivatives as dual 1H/19F MRI probes, *Chem. Commun.*, 2019, **55**, 4115–4118. DOI: 10.1039/C9CC01204D.

Abstract

Reinforced cross-bridged Ni^{2+}-cyclam complexes were functionalised with pendant arms containing both amide protons and CF_3 groups that lead to a dual $^{1}H/^{19}F$ response. The resulting complexes possess very high inertness favourable for MRI applications. The paramagnetism of the Ni^{2+} ion shifts the amide resonance 56 ppm away from bulk water favouring the chemical exchange saturation transfer (CEST) effect and shortening the acquisition times in ^{19}F magnetic resonance imaging (MRI) experiments, thus enhancing the signal-to-noise ratios compared to the fluorinated diamagnetic reference.

Magnetic resonance imaging (MRI) contrast agents (CAs) are generally paramagnetic metal complexes of Gd^{3+} able to reduce the longitudinal relaxation time (T_1) of protons in their vicinity.[1] These classical CAs are commonly used in clinical practice, although recently there have been some concerns about their toxicity.[2] This prompted the European Medicines Agency to restrict in 2017 the use of some non-macrocyclic Gd^{3+} contrast agents and suspend the authorizations for others.[3,4] Nevertheless, the use of macrocyclic Gd^{3+}-based contrast agents is thought to be safe and will likely continue in the near future.

The safety aspects and some limitations of the Gd^{3+}-based probes triggered the development of different alternatives, including: (1) developing T_1 shortening agents based on other paramagnetic metal ions such as Mn^{2+};[5] (2) the use of agents that provide contrast following the chemical exchange saturation transfer (CEST) mechanism. CEST agents contain a pool of protons in slow-to-intermediate exchange with bulk water, so that applying a radiofrequency pulse to this proton nuclei results in a decrease of the bulk water signal by saturation transfer. Paramagnetic ions such as the Ln^{3+} ions increase the chemical shift difference between the two pools of protons; consequently, the slow-to-intermediate exchange condition can be achieved with faster exchange rates.[6] Furthermore, different CEST agents based on paramagnetic transition

* david.esteban@udc.es
† carlos.platas.iglesias@udc.es

metal ions have also been proposed (Fe^{2+}, Co^{2+} and Ni^{2+}).[7] CEST agents can be activated at will by applying a radiofrequency pulse, which opens the possibility of detecting different agents simultaneously. (3) Using ^{19}F-based probes, which represent the best alternative to ^{1}H given the high sensitivity of the ^{19}F nucleus (83% with respect to ^{1}H). ^{19}F-based probes have the advantage of the negligible fluoride concentration *in vivo*, which eliminates any background signal.[8] However, ^{19}F presents rather long relaxation times (~0.6–1.5 s),[8] so that paramagnetic metal ions are used to accelerate the relaxation times and thus the acquisition times. This has been achieved both with transition metal ions[9] and lanthanides.[10]

The combination of CEST ^{1}H and ^{19}F response into a single CA may result in probes that combine the advantages of the two techniques: the generation of on/off response at will by the CEST agents and the easier quantification of the MRI signal for ^{19}F probes. Some examples of dual $^{1}H/^{19}F$ agents based on Ln^{3+} complexes were reported recently in the literature.[11] Given the potential toxicity of probes based on Ln^{3+} ions, we sought to develop transition metal complexes showing this dual output. We report here the first generation of these transition metal CA candidates based on Ni^{2+}. Stable complexation of this metal ion was achieved with the use of reinforced (cross-bridge) cyclam derivatives, functionalized with a carboxylate pendant arm to ensure a good water solubility, and including a second pendant arm containing an exchangeable amide proton for the CEST response and ^{19}F nuclei (Fig. 1).

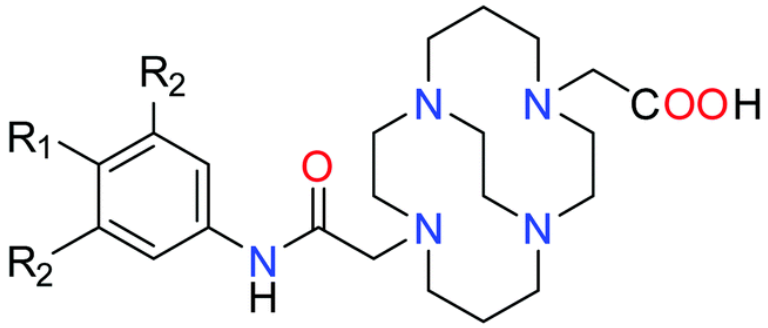

HL^1: R_1= H; R_2= CF_3
HL^2: R_1= CF_3; R_2= H

Fig. 1. Chemical structures of the ligands reported in this work.

The synthesis of the ligands was achieved by sequential alkylation of the commercially available cross-bridged precursor with *tert*-butyl bromoacetate and the chloroacetamide precursors (see ESI[i]). Hydrolysis of the *tert*-butyl groups with formic acid afforded the HL^1 and HL^2 ligands with fair overall yields (17 and 21%, respectively). The preparation of the Ni^{2+} complexes was achieved from the nitrate and trifluoromethanesulfonate salts for $[NiL^1]^+$ and $[NiL^2]^+$, respectively, and required harsh conditions due to slow complexation kinetics, using *n*-butanol as a solvent and high temperature.[12]

The structures of both complexes were determined using X-ray diffraction measurements (Fig. 2). The $[NiL^1]^+$ and $[NiL^2]^+$ complexes were crystallised as the chloride and trifluoromethanesulfonate salts, respectively. The metal ion is directly coordinated to the four N atoms of the macrocyclic unit, with Ni–N distances in the range of 2.07–2.10 Å. These values fall in the low part of the range observed for the few cross-bridged Ni^{2+} complexes reported in the literature (2.09–2.20 Å).[13] The oxygen atoms of the pendant arms complete the distorted octahedral coordination around the metal ion in both cases. The Ni–O distance

involving the carboxylate oxygen atom (2.026 Å for $[NiL^1]^+$ and 2.058 Å for $[NiL^2]^+$) is slightly shorter than that of the amide oxygen atom (2.075 Å and 2.110 Å for $[NiL^2]^+$ and $[NiL^1]^+$, respectively). The macrocyclic unit adopts a *cis*-V conformation, with the bicyclo[6.6.2] ligand units adopting [2323] conformations, as usually observed for complexes of cross-bridged cyclam derivatives with small metal ions.[14]

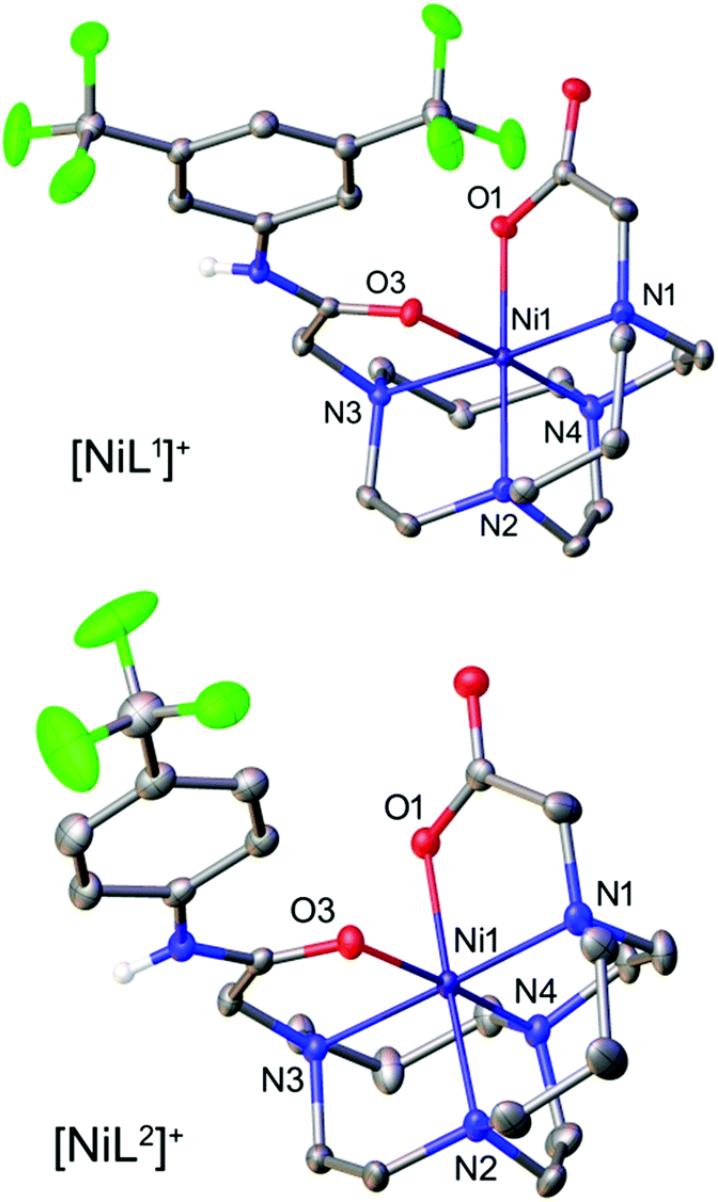

Fig. 2. The X-ray crystal structure of the $[NiL^1]^{2+}$ and complexes. Bond distances (Å): $[NiL^1]^+$ Ni–O3 2.075(2); Ni–O1 2.026(1); Ni–N1 2.084(2); Ni–N2 2.071(2); Ni–N3 2.097(2); Ni–N4 2.070(2). $[NiL^2]^+$: Ni–O1 2.0579(18); Ni–O3 2.1103(18); Ni–N1 2.083(2); Ni–N2 2.082(2); Ni–N3 2.096(2); Ni–N4 2.068(2).

The inertness of the $[NiL^1]^+$ complex was assessed by using spectrophotometric measurements. The absorption spectrum of a 4 M HCl solution of the complex presents a maximum at 248 nm due to the phenylamide chromophore. The absorption spectrum recorded after 24 h is identical to that recorded immediately after dissolving the complex. Furthermore, the mass spectrum of the solution obtained with electrospray ionisation presents the peak of the $[NiL^1]^+$ entity at m/z = 542.19, while the peak of the protonated ligand at m/z = 486.26 was not observed (Fig. 3). These results confirm that the complex is inert

under these harsh conditions. For instance, the $[Gd(DOTA)]^-$ complex, which is used as a contrast agent in clinical practice as DOTAREM®, undergoes dissociation under these conditions with a half-life of 144 minutes.[15]

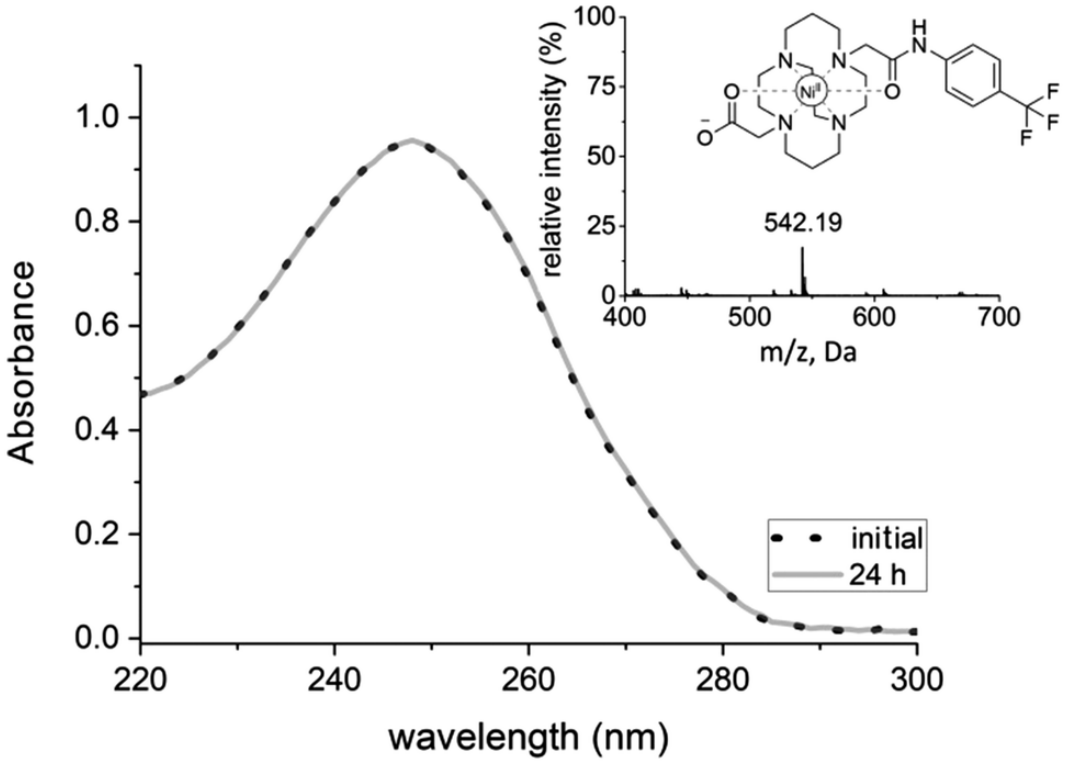

Fig. 3. The UV-vis spectra of a 5.2×10^{-5} M fresh aqueous solution of $[NiL^2]^+$ and that of the same solution registered 24 h later (25 °C, 4 M HCl). Inset: Experimental ESI-MS spectrum of the $[NiL^2]^+$ complex recorded in strongly acidic conditions after 5 days.

The two Ni^{2+} complexes provide moderate CEST effects. The measurements were carried out using 15 mM H_2O solutions of the complexes containing 20% acetonitrile due to their low solubility in pure water (Fig. 4). The CEST spectra present prominent CEST peaks at 56 ppm and 25 °C in both complexes due to the amide proton of the ligands, while the shift reduces to ~52 ppm when the spectra were recorded at 37 °C. This chemical shift is somewhat smaller than those observed for the Ni^{2+} complexes with ligands containing acetamide[7c,16] (typically ~70 ppm) or picolinamide[17] groups (~85 ppm). The CEST spectra obtained with different saturation powers were quantitatively analysed using the standard Bloch-McConnell equations and 2 exchanging pools (paramagnetically shifted pool and bulk water),[18] providing exchange rates of amide protons of k_{ex} = 10.9 ± 1.1 and 7.1 ± 1.7 kHz for $[NiL^1]^+$ and $[NiL^2]^+$, respectively. The exchange of amide protons generally follows a base-catalysed mechanism.[17] Thus, the higher rate determined for $[NiL^1]^+$ is likely related to the more acidic character of the amide proton due to the combined electron withdrawing effect of two CF_3 substituents. However, given the fast exchange rates of both complexes already at 25 °C and the low solubility of the complexes in water, further structural adjustments would be necessary to optimise their properties for potential use as CEST MRI contrast agents (*i.e.* by incorporating the CF_3 groups on the carbon atoms of the macrocycle at the β-N position or the methylenic carbon atoms of the pendant arms).[19]

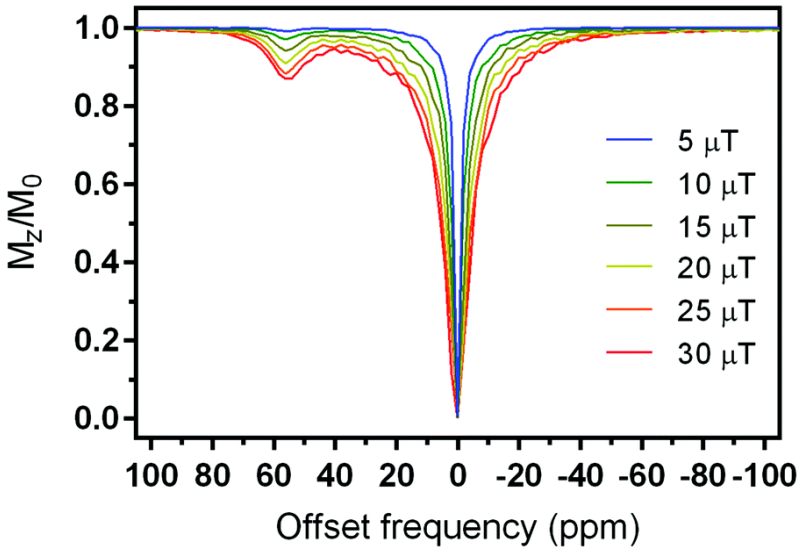

Fig. 4. The CEST spectra of $[NiL^2]^+$ (15 mM) in H_2O containing 20% acetonitrile (pH 7, saturation time 10 s) recorded using different saturation powers.

The ^{19}F NMR spectra of the two complexes present a signal at −59.7 ppm due to the ligand CF_3 groups, which in the case of $[NiL^1]^+$ implies that the rotation about the amide N–C bond of the phenyl group is fast on the NMR time scale. The spectra of the two complexes show very different linewidths, which anticipates distinct ^{19}F relaxation rates (Fig. 5). This is confirmed by the longitudinal (R_1) and transverse (R_2) relaxation rates, which were measured at three different magnetic fields (Table 1 and Fig. 5). Both the R_1 and R_2 values remain constant within the experimental error at 7, 9.4 and 11.75 T. The two complexes present virtually identical R_1/R_2 ratios (Table 1). Both the R_1 and R_2 values are higher for $[NiL^1]^+$ with respect to $[NiL^2]^+$, which is likely associated with a shorter average Ni···F distance in the former. The experimental data were analysed using the standard Solomon–Bloembergen–Morgan theory of paramagnetic relaxation.[20] The ^{19}F relaxation rates at the high fields employed in this study are not affected by the relaxation of the Ni^{2+} electron spin. Thus, the analysis of the experimental data required fitting two parameters: the rotational correlation time τ^{298}_R, which was assumed to be identical for the two complexes, and the Ni···F distances. We obtained a τ^{298}_R value of the Ni···F vector of 89 ± 10 ps, which is reasonable considering the size of the complexes. The Ni···F distances were determined to be 7.28 ± 0.42 and 8.72 ± 0.5 Å for $[NiL^1]^+$ and $[NiL^2]^+$, respectively. The dipolar paramagnetic relaxation mechanism is proportional to $(1/r_{NiF})^6$, with r_{NiF} being the Ni···F distance. The r_{NiF} distances estimated by averaging the $(1/r_{NiF})^6$ values observed in the X-ray crystal structures of the $[NiL^1]^+$ and $[NiL^2]^+$ are 7.0 and 9.3 Å, respectively. Thus, the values obtained from the analysis of relaxation data and those estimated from the X-ray structures are in good mutual agreement.

Table 1. ^{19}F longitudinal (R_1) and transverse (R_2) relaxation rates obtained from 15 mM aqueous solutions of $[NiL^1]^+$ and $[NiL^2]^+$ containing 20% acetonitrile and signal-to-noise ratios (SNRs) obtained with phantom MRI studies (25 °C, 7.05 T)[a].

Complex	R_1 (s^{-1})	R_2 (s^{-1})	R_1/R_2	SNR
$[NiL^1]^+$	99.4(1)	125.0(2)	0.80	136.9/47.8[b]
$[NiL^2]^+$	34.2(1)	40.8(2)	0.84	98.3/30.0[b]

[a] Data obtained at 7.05 T. Standard deviations within parenthesis.
[b] SNRs obtained for TFA using identical experimental conditions.

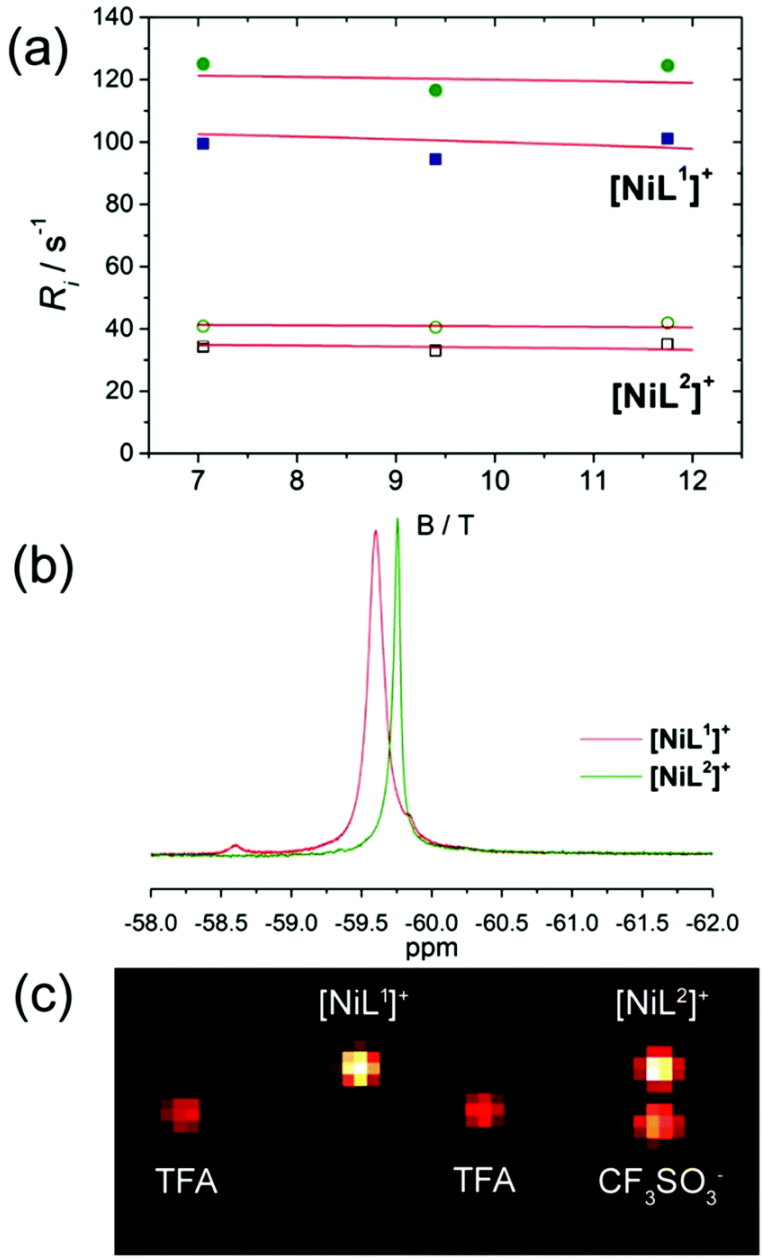

Fig. 5. (a) Top: longitudinal (R_1, squares) and transverse (R_2, circles) relaxation rates recorded for $[NiL^1]^+$ and $[NiL^2]^+$ (as the chloride and triflate salts, respectively). The solid lines correspond to the fits of the data using Solomon–Bloembergen–Morgan theory. (b) ^{19}F NMR spectra (7.05 T, 25 °C) of $[NiL^1]^+$ and $[NiL^2]^+$. (c) ^{19}F MRI on tube phantoms (15 mM complex, 7.05 T, RT) of $[NiL^1]^+$, $[NiL^2]^+$ and TFA (30 mM left tube, 15 mM right tube). Acquisition parameters: FOV = 32 × 32, MTX = 32 × 32, slice thickness 5 mm, pixel size 1 mm, 400 µL vials.

We also undertook a ^{19}F MRI study on tube phantoms using 15 mM solutions of the two complexes. Tubes containing trifluoroacetic acid (TFA) with equal ^{19}F nuclei concentrations (*i.e.* 30 and 15 mM of TFA relative to $[NiL^1]^+$ and $[NiL^2]^+$, respectively) were used for comparative purposes. The tube containing $[NiL^2]^+$ resulted in the 'ghost' image arising from the presence of trifluoromethanesulfonate counter anions (see above),[8] which did not affect the SNR for $[NiL^2]^+$ due to sufficient difference in the resonance frequency of fluorine atoms in these two molecules. The resulting ^{19}F MR images confirmed the potential of these complexes as ^{19}F probes. The obtained signal-to-noise ratio (SNR) for $[NiL^1]^+$ after 1 hour acquisition time was 137, which was 2.8 times higher than that of TFA (48). Concurrently, the SNR determined for $[NiL^2]^+$ was 3.3 times higher than that of TFA. Obviously, the paramagnetism of the metal ion affected the ^{19}F relaxation times to a significant extent; however, proportional shortening of both ^{19}F T_1 and T_2 resulted in

values that allow fast repetitions with still sufficient signal, thus giving rise to greater SNR values. In turn, these ^{19}F MRI experiments demonstrated advantageous properties of $[NiL^1]^+$ and $[NiL^2]^+$ over the diamagnetic reference, indicating perspectives for their consideration as ^{19}F MRI contrast agents.

In conclusion, we have reported Ni^{2+} cross-bridged derivatives that form extremely inert complexes with great potential for the design of MRI probes. We demonstrated that functionalisation of the macrocyclic platform with pendant arms containing amide protons and CF_3 groups provides potential for these systems to be used as $^1H/^{19}F$ probes. The paramagnetism of the Ni^{2+} ion allows for a faster ^{19}F MRI acquisition thanks to the paramagnetic relaxation enhancement effect. The paramagnetically shifted resonance of amide protons promotes the CEST effect safely distant from bulk water. This work further expands the scope of applications of the cyclam-based systems, ensuring exciting forthcoming developments in the field of chemistry of MRI contrast agents.

Authors R. P.-P., D. E.-G. and C. P.-I. thank Ministerio de Economía y Competitividad (CTQ2016-76756-P) and Xunta de Galicia (ED431B 2017/59 and ED431D 2017/01) for generous financial support. R. P.-P. thanks Ministerio de Economía y Competitividad for a PhD FPI grant (BES-2014-068399) and a fellowship for a short term stay in Tuebingen (EEBB-I-17-12213). T. S. thanks the German Academic Exchange Service (DAAD) for the PhD fellowship.

Conflicts of interest

There are no conflicts to declare.

References

01 (*a*) *The Chemistry of Contrast Agents in Medical Magnetic Resonance Imaging*, A. E. Merbach, L. Helm and E. Toth, John Wiley & Sons Ltd, 2013; (*b*) L. Helm, J. R. Morrow, C. J. Bond, F. Carniato, M. Botta, M. Braun, Z. Baranyai, R. Pujales-Paradela, M. Regueiro-Figueroa, D. Esteban-Gómez, C. Platas-Iglesias and T. J. Scholl, *Contrast Agents for MRI: Experimental Methods*, V. C. Pierre and M. J. Allen, The Royal Society of Chemistry, 2017, pp. 121–242.

02 (*a*) D. R. Roberts, S. M. Lindhorst, C. T. Welsh, K. R. Maravilla, M. N. Herring, K. A. Braun, B. H. Thiers and W. C. Davis, *Invest. Radiol.*, 2016, **51**, 280; (*b*) M. Birka, K. S. Wentker, E. Lusmöller, B. Arheilger, C. A. Wehe, M. Sperling, R. Stadler and U. Karst, *Anal. Chem.*, 2015, **87**, 3321; (*c*) E. Kanal and M. F. Tweedle, *Radiology*, 2015, **275**, 630; (*d*) T. J. Fraum, D. R. Ludwig, M. R. Bashir and K. J. Fowler, *J. Magn. Reson. Imaging*, 2017, **46**, 338.

03 (*a*) S. Cheng, L. Abramova, G. Saab, G. Turabelidze, P. Patel, M. Arduino, T. Hess, A. Kallen and M. Jhung, *J. Am. Med. Assoc.*, 2007, **297**, 1542; (*b*) T. H. Darrah, J. J. Prutsman-Pfeiffer, R. J. Poreda, M. E. Campbell, P. V. Hauschka and R. E. Hannigan, *Metallomics*, 2009, **1**, 479.

04 V. M. Runge *Invest. Radiol.*, 2018, **53**, 571.

05 E. M. Gale, I. P. Atanasova, F. Blasi, I. Ay and P. Caravan, *J. Am. Chem. Soc.*, 2015, **137**, 15548.

06 (*a*) S. J. Ratnakar, M. Woods, A. J. M. Lubag, Z. Kovacs and A. D. Sherry, *J. Am. Chem. Soc.*, 2008, **130**, 6; (*b*) S. J. Ratnakar, T. C. Soesbe, L. L. Lumata, Q. N. Do, S. Viswanathan, C.-Y. Lin, A. D. Sherry and Z. Kovacs, *J. Am. Chem. Soc.*, 2013, **135**, 14904.

07 (*a*) S. J. Dorazio, P. B. Tsitovich, K. E. Siters, J. A. Spernyak and J. R. Morrow, *J. Am. Chem. Soc.*, 2011, **133**, 14154; (*b*) P. B. Tsitovich, J. A. Spernyak and J. R. Morrow, *Angew. Chem., Int. Ed.*, 2013, **52**, 13997; (*c*) A. Olatunde, S. J. Dorazio, J. A. Spernyak and J. R. Morrow, *J. Am. Chem. Soc.*, 2012, **134**, 18503.

08 J. Ruiz-Cabello, B. P. Barnett, P. A. Bottomley and J. W. Bulte, *NMR Biomed.*, 2011, **24**, 114.

09 (*a*) J. Blahut, P. Hermann, A. Gálisová, V. Herynek, I. Císařová, Z. Tošnerc and J. Kotek, *Dalton Trans.*, 2016, **45**, 474; (*b*) M. Yu, D. Xie, K. P. Phan, J. S. Enriquez, J. J. Luci and E. L. Que, *Chem. Commun.*, 2016, **52**, 13885; (*c*) J. Blahut, K. Bernasek, A. Galisova, V. Herynek, I. Cisarova, J. Kotek, J. Lang, S. Matejkova and P. Hermann, *Inorg. Chem.*, 2017, **56**, 13337.

10 (*a*) K. L. Peterson, K. Srivastava and V. C. Pierre, *Front. Chem.*, 2018, **6**, 160; (*b*) K. Srivastava, E. A. Weitz, K. L. Peterson, M. Marjanska and V. C. Pierre, *Inorg. Chem.*, 2017, **56**, 1546–1557; (*c*) K. H. Chalmers, E. De Luca, N. H. M. Hogg, A. M. Kenwright, I. Kuprov, D. Parker, M. Botta, J. I. Wilson and A. M. Blamire, *Chem. – Eur. J.*, 2010, **16**, 134.

11 N. Cakić, T. Savić, J. Stricker-Shaver, V. Truffault, C. Platas-Iglesias, C. Mirkes, R. Pohmann, K. Scheffler and G. Angelovski, *Chem. Commun.*, 2016, **136**, 17954.

12 A. Rodriguez-Rodriguez, D. Esteban-Gomez, R. Tripier, G. Tircso, Z. Garda, I. Toth, A. de Blas, T. Rodriguez-Blas and C. Platas-Iglesias, *J. Am. Chem. Soc.*, 2014, **54**, 10056.

13 (*a*) R. Smith, D. Huskens, D. Daelemans, R. E. Mewis, C. D. Garcia, A. N. Cain, T. N. C. Freeman, C. Pannecouque, E. De Clercq, D. Schols, T. J. Hubin and S. J. Archibald, *Dalton Trans.*, 2012, **41**, 11369; (*b*) D. G. Jones, K. R. Wilson, D. J. Cannon-Smith, A. D. Shircliff, Z. Zhang, Z. Chen, T. J. Prior, G. Yin and T. J. Hubin, *Inorg. Chem.*, 2015, **54**, 2221–2234.

14 (*a*) M. Meyer, V. Dahaoui-Gindrey, C. Lecomte and R. Guilard, *Coord. Chem. Rev.*, 1998, **178–180**, 1313; (*b*) J. Dale *Acta Chem. Scand.*, 1973, **27**, 1115.

15 E. Toth, E. Brucher, I. Lazar and I. Toth, *Inorg. Chem.*, 1994, **33**, 4070.

16 A. O. Olatunde, C. J. Bond, S. J. Dorazio, J. M. Cox, J. B. Benedict, M. D. Daddario, J. A. Spernyak and J. R. Morrow, *Chem. – Eur. J.*, 2015, **21**, 18290.

17 L. Caneda-Martínez, L. Valencia, I. Fernández-Pérez, M. Regueiro-Figueroa, G. Angelovski, I. Brandariz, D. Esteban-Gómez and C. Platas-Iglesias, *Dalton Trans.*, 2017, **46**, 15095.

18 M. Zaiss, G. Angelovski, E. Demetriou, M. T. McMahon, X. Golay and K. Scheffler, *Magn. Reson. Med.*, 2018, **79**, 1708.

19 (*a*) N. Camus, Z. Halime, N. Le Bris, H. Bernard, C. Platas-Iglesias and R. Tripier, *J. Org. Chem.*, 2014, **79**, 1885; (*b*) W. Liu, G. Hao, M. A. Long, T. Anthony, J.-T. Hsieh and X. Sun, *Angew. Chem., Int. Ed.*, 2009, **48**, 7346.

20 (*a*) I. Solomon and N. Bloembergen, *J. Chem. Phys.*, 1956, **25**, 261; (*b*) N. Bloembergen and L. O. Morgan, *J. Chem. Phys.*, 1961, **34**, 842.

[i] Electronic supplementary information (ESI) available: Synthetic procedures and experimental details. CCDC 1891730 and 1891731. For ESI and crystallographic data in CIF or other electronic format see DOI: 10.1039/c9cc01204d.